Cristical raw material-free catalysts and electrocatalysts: complementary strategies to activate economic, robust, and ecofriendly SrTiO3

Giovanni Carollo, Alberto Garbujo, Fabrice Mauvy, Antonella Glisenti

Critical raw material-free catalysts and electrocatalysts: complementary strategies to active economic, robust, and ecofriendly $SrTiO_3$.

Giovanni Carollo,[a] Alberto Garbujo,[a] Fabrice Mauvy,[b] Antonella Glisenti[a,c,*]

a Dept. of Chemical Sciences - University of Padova - Via Marzolo, 1 35131 Padova, Italy

b CNR- ICMATE - Via Marzolo, 1 35131 Padova, Italy

c CNRS - Université de Bordeaux, ICMCB, 87 - Av. Dr. Schweitzer, F-33608 Pessac Cedex, France.

KEYWORDS: titanates, functional ceramics, electrocatalysis, catalysis, SOFC, dry reforming.

ABSTRACT: In this contribution new $SrTiO_3$ based advanced materials have been developed and their catalytic and electro catalytic properties have been tuned by means of the following strategies: doping, nano composition, infiltration. The aim is in developing highly functional materials within a Critical Raw Material-free approach with a particular aim toward durability at high temperature and tolerance to C-poisoning. In spite of the absence of catalytic and electro catalytic properties, we started from a very economic and durable perovskite, of $SrTiO_3$-type, because of its high stability also under reducing conditions with the aim of implementing performances with insertion of Ba and Mo into the crystalline cell. The catalysts are of the type $Ba_xSr_{1-x}Ti_{1-y}Mo_yO_3$, with x = 0 and 0.5, y = 0, 0.1 and 0.4. Starting from traditional wet chemistry procedure a new synthesis method was developed to obtain high purity and control molybdenum insertion into perovskite lattice. This result has been successfully obtained by means of a detailed characterization carried out during each preparation steps by means of XRD, XPS, SEM, EDX, TPD, TPR, BET. Characterization results allowed also to go deeper into the properties of the developed materials and to drive the enhancement of the catalytic and electro catalytic performances. At these purposes, the catalytic (CO oxidation and CH_4 dry reforming) and electro catalytic (as anode in Solid Oxide Fuel Cells) activity was studied and the effect of activation with nickel nano deposition was investigated. Electro catalytic activity was studied by means of Electrochemical Impedance Spectroscopy in symmetric cells obtained using Yttria Stabilized Zirconia (YSZ) as electrolyte and a Cerium Gadolinium Oxide (CGO) buffer layer. In this case Ni impregnation was preferred. Summarizing we demonstrated that starting from an economic, sustainable and robust material, several functional properties (catalytic and electro catalytic activity) can be developed. We obtained a good catalyst for Methane Dry Reforming and CO oxidation and a good anode for Solid Oxide Fuel Cells. Both in catalysis and electro catalysis the effect of Ni is relevant.

INTRODUCTION

Several materials exhibit high performance (particularly in catalytic and electro catalytic applications) mainly due to the presence of noble metals. Our aim is in developing these functionalities while avoiding noble metals in a Critical Raw Materials (CRM)-free approach. In this contribution new $SrTiO_3$ based perovskites with enhanced catalytic and electro catalytic performance, have been obtained by doping with Ba, and Mo.

In fact, we are convinced that the strategies we applied can have a wide application when high performance and economic, environmental sustainability are request.

$SrTiO_3$ systems are characterized by good stability at high temperatures under severe reducing and oxidizing conditions and by a low environmental and economic impact. Beside for their stability, titanates are interesting for superconductivity [1] and photo catalysis [2-3] as an example. $SrTiO_3$ is not characterized by high conductivity or catalytic activity: with the present contribution we demonstrate that these properties can be greatly enhanced through a suitable doping, nano composition, and nano-infiltration. We expect catalytic activity to be enhanced by doping in the B-site with a transition metal capable of creating a redox couple;[4-5] in a similar way the electrocatalytic activity can be increased. [6-9] The insertion of Ba in La1-xSrxTiO3 is reported not to affect the chemical stability of the compound and, at the same time, to improve the activity when H_2S is present in H_2 and CH_4 feed [10] so we decided to insert this element with the aim of studying its effect of stability and tolerance to C-poisoning.

Molybdenum is considered interesting in the fields of catalysis and electro catalysis. Molybdates, especially $SrMoO_3$ and $BaMoO_3$, have the highest electronic conductivity (about 10^4 S/cm at 25°C) among ceramic materials. Moreover, molybdenum oxides (MoO_2) are good hydrocarbons reforming catalysts with no carbon poisoning. [11]. Molybdenum is characterized by a big ionic radius and the tendency to be stable in high oxidation states (+4, +6): strong reducing treatments are thus usually required to obtain the correct phase [12]. Titanium doped molybdates have been studied as a possible solution to the chemical instability under working conditions (Mo) and the low electronic conduction (Ti) [13].

Further conductivity and reactivity have been reached building nanocomposites with Ni using wet impregnation (for catalysis application) and infiltration (for electro catalysis application). All titanates have been prepared by a wet chemistry procedure: the citrate route capable of allowing the formation of homogeneous phases; wet impregnation was preferred as a starting point, for the nanocomposites because it a preparation procedure, easy to be carried out and up-scaled and allows the deposition of the desired amount of supported material. By infiltration, nano-sized particles with high surface areas and improved electro catalytic behaviour are obtained. The advantage of the infiltration technique is the homogeneous mixing of the cations and the low calcination temperatures required; lower temperature allow avoiding cation interdiffusion between electrode and electrolyte during the cell preparation.[14]

Following above considerations we decided for the opposite strategy by developing Mo- (testing the increasing amount of Mo) and Ba,Mo-doped titanates with the aim of improving catalytic and electro catalytic properties while keeping the stability and robustness of $SrTiO_3$:

1. $SrTi_{0.9}Mo_{0.1}O_3$,
2. $SrTi_{0.6}Mo_{0.4}O_3$,
3. $Ba_{0.5}Sr_{0.5}Ti_{0.9}Mo_{0.1}O_3$,
4. $NiO(0.3)/ SrTi_{0.9}Mo_{0.1}O_3$
4. $NiO(0.3)/ SrTi_{0.6}Mo_{0.4}O_3$

The characterization of the prepared compounds was carried out by means of X-Ray Diffraction (XRD), X-Ray Photoelectron Spectroscopy (XPS), Scanning Electron Microscopy (SEM), Energy Dispersive X-Ray Spectroscopy (EDX), BET, Temperature Programmed Reduction and Desorption (TPR, TPD). The results of the characterization, with particular reference to the XRD, have been the base for the development and optimization of the synthesis procedure.

The catalytic activity was studied in two strategic probe reactions: CO oxidation and methane dry reforming; the electro catalytic behaviour was investigated testing the material as anode of a Solid Oxide Fuel Cell (SOFC). The possibility to address catalytic and electro catalytic activity by using nano decoration approach has been investigated considering nickel as dispersed active specie.

RESULTS AND DISCUSSION

Characterization: Structure investigation (XRD)

The synthesis procedures have been optimized for each sample as reported in Supporting Information.

Figure 1a, displays the diffraction patterns of $SrTi_{0.9}Mo_{0.1}O_3$. If the thermal treatment is carried out in air an undesired insulator phase, $SrMoO_4$, forms in addition to $SrTiO_3$.

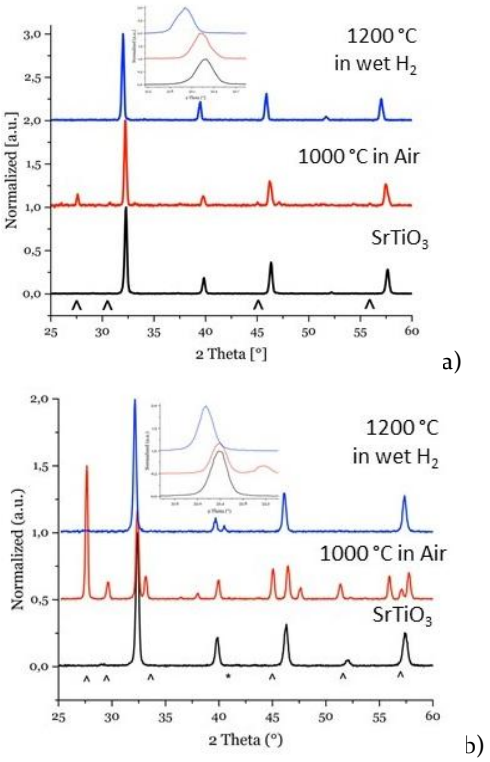

Figure 1 a) XRD patterns of a) $SrTi_{0.9}Mo_{0.1}O_3$ and b) $SrTi_{0.6}Mo_{0.4}O_3$ after different treatments. (^) $SrMoO_4$ (tetragonal) 01-085-0586 JCPDS database (*) Mo(0) (cubic) 00-042-1120 JCPDS database $SrTiO_3$ (cubic) 00-040-1500 JCPDS database

Table 1: Thermal treatments, pre-treatments, and environmental condition carried out for optimizing the synthesis procedure for Mo and Ba doped titanates.

Composition	Pre-Treatments	Thermal treatment			Correct Phase
		[°C]	Environment	[h]	
$SrTi_{0.9}Mo_{0.1}O_3$	400 °C, 2 h Air	1000	Air	6	No
	400 °C, 2 h Air	850	Air	6	No
	400 °C, 2 h Air	850	H_2	6	No
	400 °C, 2 h Air	1000	5% H_2/Ar	6	Yes with Mo impurity
	No	1000	5% H_2/Ar	6	Yes with Mo impurity
	No	1000	20% H_2/Ar	6	Yes with Mo impurity
	No	1000	5% H_2/Ar wet	6	Yes with trace of impurity
	400 °C, 2 h Air	1000	5% H_2/Ar wet	6	Yes with trace of impurity
	No	1000	5% H_2/Ar wet	12	Yes with trace of impurity
	No	1200	5%H_2/Ar wet	6	Yes
$SrTi_{0.6}Mo_{0.4}O_3$	No	1000	Air	6	No
	No	1000	5% H2/Ar	6	Yes with Mo impurity
	No	1000	5% H2/Ar wet	6	Yes with trace of Mo impurity
	No	1200	5%H2/Ar wet	6	Yes with trace of Mo impurity
$Ba_{0.5}Sr_{0.5}Ti_{0.9}Mo_{0.1}O_3$	400 °C, 2 h Air	1000	Air	6	No
	400 °C, 2 h Air	1000	5% H_2/Ar	6	No
	400 °C, 2 h Air	1000	% H_2/Ar wet	6	No
	No	1000	5% H_2/Ar wet	6	Yes with trace of Mo impurity
	No	850	5% H_2/Ar Ethanol	6	No
	No	1000	5% H_2/Ar Ethanol	6	Yes with impurity
	No	1000	5% H_2/Ar Ethanol/water 50% vol	6	Yes

This phase is observed to segregate during the synthesis at low temperature [15-17]; to avoid its formation, specific conditions for thermal treatment have been compared and optimized (Table 1). The best result was obtained by heating in 5%H2+H2O environment. Treatments in air always give rise to the insulant impurity phase while reduction is too strong without water, favouring the formation of elemental molybdenum outside the perovskite cell.

In 5%H2+H2O, taking into consideration the $SrTiO_3$ reference pattern, a small shift to lower angle can be observed in the Mo-doped $SrTiO_3$ confirming the insertion in the perovskite cell with Ti substitution. No significant effect has a pre-treatment at 400 °C carried out to gradually eliminate the organic residuals.

Also in $SrTi_{0.6}Mo_{0.4}O_3$ (Figure 1b) as in $SrTi_{0.9}Mo_{0.1}O_3$, the thermal treatment in air induces the formation of $SrMoO_4$ and a treatment under reducing conditions is necessary. In this last case, the XRD pattern of $SrTi_{0.6}Mo_{0.4}O_3$ obtained in 5%H2+H2O, revealed a small segregation of Mo(0) at 40.5°.

Figure 2 shows the patterns after the thermal treatment carried out on $Ba_{0.5}Sr_{0.5}Ti_{0.9}Mo_{0.1}O_3$. The successful substitution of Sr with Ba in $SrTi_{0.9}Mo_{0.1}O_3$ required the accurate optimization of pO2 conditions: the treatment in air, in fact, induces the oxidation of Mo(IV) to Mo(VI) with a segregation of secondary phases ($BaMoO_4$, BaO, MoO_3), while a reductive treatment in 5%H2 dry and wet conditions induces the formation of Mo(0) and $BaMoO_4$/BaO, MoO_3, respectively. The optimized conditions to obtain the material were achieved by flowing 5% H_2/Ar in a mixture of 50% Ethanol in H2O so enhancing the reductant power of the environment, as also observed in the synthesis of MoO2 from MoO3 [18].

Stability under oxidizing and reducing conditions

Once obtained the insertion of dopants inside the perovskite crystalline cell it is fundamental to evaluate the effect of doping on the stability. According to literature, [19] titanium based perovskites do not show any reduction peak: the absence of signal in the TPR curves of the Mo-doped titanates confirms that Mo(IV) is stabilized by introduction into the perovskite structure. In fact, Bhaskar et al. [20] observed the reduction from Mo(VI) to Mo (IV) at 767°C and the reduction of Mo(IV) to Mo(0) at 987°C; we did not observe these contributions.

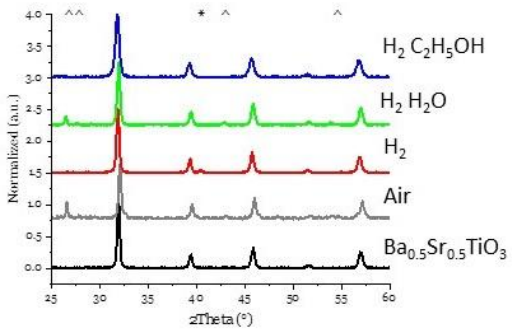

Figure 2: XRD patterns of a) Ba0.5Sr0.5Ti.9Mo0.1O3 obtained after different treatments.
(^) BaMoO4 / BaO, MoO3 (tetragonal) 00-029-0193 JCPDS database;
(*) Mo(0) (cubic) 00-042-1120 JCPDS database;
Ba0.5Sr0.5TiO3 (cubic) 00-039-0039 JCPDS database.

The temperature programmed oxidation (TPO) was carried out with the purpose to investigate the stability of Mo-doped titanates under oxidising condition.

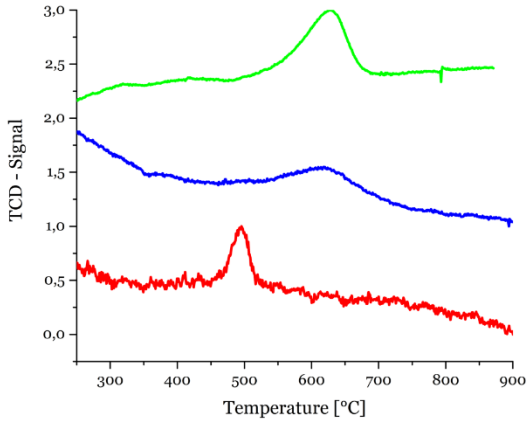

Figure 3: Temperature programmed oxidation on $SrTi_{0.9}Mo_{0.1}O_3$ (red), $SrTi_{0.6}Mo_{0.4}O_3$ (blue), and $Ba_{0.5}Sr_{0.5}Ti_{0.9}Mo_{0.1}O_3$.

TPO results (Figure 3) suggest that Mo-doped titanates are susceptible to oxidising atmosphere. In SrTi0.9Mo0.1O3 a narrow peak at 497 °C indicates the one step oxidation of Mo(IV) to Mo(VI) and the consequent formation of SrMoO4. The redox signal is in agreement with literature in which thermo gravimetric analysis shown the oxidation of Mo(IV) to Mo(VI) between 500 °C and 700 °C [21-22]. This was also confirmed by the XRD pattern, Figure 4, carried out after TPO. The same redox behaviour was observed in SrTi0.6Mo0.4O3 and Ba0.5Sr0.5Ti0.9Mo0.1O3 displaying two broad peaks at 621 °c and 629 °C, respectively. The higher temperature required for Mo(IV) oxidation suggested a higher cation stability. The broad peaks shape could be explained by the traces of Mo metal on SrTi0.6Mo0.4O3, visible in figure 3.2 at 40.5°, and by the presence of MoO2 observed with XPS analysis. The %O2 consumption data, reveal only a partial oxidation of Mo(IV) to Mo(VI) suggesting the stability of Mo(IV) in the SrTiO3 structure. Ba greatly decrease O2 consumption. With respect to the total Mo, 27.9% is oxidized for Ba0.5Sr0.5Ti0.9Mo0.1O3, compared with 45.3% for SrTi0.9Mo0.1O3 (60.9% for SrTi0.6Mo0.4O3). Ba seems to stabilize Mo(IV) with respect to oxidation. In order to confirm TPO data interpretation, XRD analyses were performed after TPO. The oxidation of elemental Mo to MoO3 also contributes to the O2 consumption detected for SrTi0.6Mo0.4O3.

The XRD patterns after TPO, figure 4, show the presence of small amounts of BaMoO4 (in Ba0.5Sr0.5Ti0.9Mo0.1O3) and SrMoO4 (in SrTi0.6Mo0.4O3 and SrTi0.9Mo0.1O3. With the purpose of testing the reversibility of the molybdenum oxidation, TPR after TPO were performed and the phases were checked by XRD. SrTi0.9Mo0.1O3 has shown a complete structure restoration; SrTi0.6Mo0.4O3 and Ba0.5Sr0.5Ti0.9Mo0.1O3 kept only trace of secondary phases. The observed impurities are electrical insulators but, the reductive environment under SOFC's anode working condi-

tions is expected to avoid their formation; moreover, as observed, their formation is reversible. [15-17]

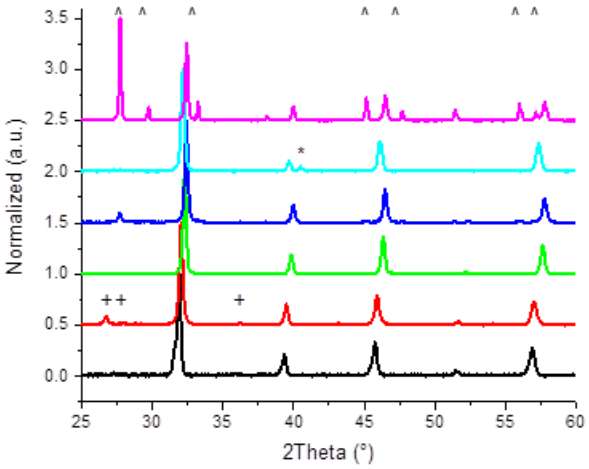

Figure 4: XRD patterns of BaySr1-yTi1Mo1-xO3 before and after TPO. From Low to High: Ba0.5Sr0.5Ti0.9Mo0.1O3, Ba0.5Sr0.5Ti0.9Mo0.1O3 after TPO; SrTi0.9Mo0.1O3, SrTi0.9Mo0.1O3 after TPO, SrTi0.6Mo0.4O3, SrTi0.6Mo0.4O3 after TPO
(*) Mo(0) (cubic) 00-042-1120 JCPDS database;
(^) $SrMoO_4$ (tetragonal) 01-085-0586 JCPDS database
(+) $BaMoO_4$ / BaO, MoO_3 (tetragonal) 00-029-0193 JCPDS database.

Surface characterization

The XP spectra are reported in figure S1. Sr 3d XPS signal shows two peaks centred at 134.7-134.8 eV and 132.2-132.5 eV. The fitting procedure suggests the overlap of two doublets attributed, in according with literature, to the perovskite (133.8-132.2 eV) and to SrO/Sr(OH)2 (134.9 eV and 133.6) 23-25] The Ti 2p3/2 XPS peak position 458.6-458.4 eV agrees with how expected for titanium in $SrTiO_3$ and $BaTiO_3$ [25]. The Ti 2p signal on sample Ba0.5Sr0.5Ti0.9Mo0.1O3 shows a contribution at 460.5 eV suggesting a higher hydroxylation. The asymmetric Ba 3d 5/2 XPS signal is centred at 779.4 eV which is characteristic for Ba in $BaTiO_3$. The shoulder observed at high BE is due to the contribution of $BaCO_3$ (typically at 779.1 eV) and to Ba(OH)2 (779.3 eV) [26,27].
The signal Mo 3d centred at 235.5-235.6 eV and 232.5 eV revealed the presence of Mo(VI) and Mo (IV) The Mo(VI)/Mo(IV) ratio is 0.7 in SrTi0.9Mo0.1O3, 0.85 in SrTi0.6Mo0.4O3 and 2.0 in Ba0.5Sr0.5Ti0.9Mo0.1O3. This difference is not related to the Goldschmidt tolerance factor, which is not significantly affected by the oxidation state of Mo, but probably to the different preparation conditions [28-30]. Focussing on the O 1s XPS peak, spectra reveal two contributions: one (529.6 eV) is due to lattice oxygen whereas the other one (about 531.8 eV) suggests the presence of hydroxide species, such as Ba(OH)2 and non-perovskitic oxides (MoO_3 and TiO_2) [31-33].

The XPS quantitative analysis of Mo-doped titanates is reported in table 2. For a comparison the samples $SrTiO_3$ and Sr0.5Ba0.5TiO3 were prepared trough citrates' synthesis and treated under the same reductive atmosphere used for Mo-doped titanates. All the samples are characterized by surface oxygen over stoichiometry confirming the presence of OH-terminations. This is relevant because OH-groups are Brønsted acidic groups that can evolve into Lewis surface active acidic groups under thermal treatment. Lewis surface acidic sites can greatly enhance the CO and CO_2 coordination so increasing the reactivity. In the undoped $SrTiO_3$ the surface segregation of titanium is observed. This behaviour disappears when Mo is inserted: in this case Sr is surface segregated in the sample with lower amount of dopant and Mo tends to surface segregate when present in higher amount. Sr is also surface segregated in Ba0.5Sr0.5TiO3 but this phenomenon is not anymore observed when also Mo is added.

The presence of large ion Ba^{2+} in Ba0.5Sr0.5Ti0.9Mo0.1O3 keeps the cation concentration close to the nominal value. An interesting contribution of H.I. Yoo et al. [34] underline the equal mobility of constituent cations in $BaTiO_3$ and thus the absence of compositional demising. Studies carried out on Ba1-xSrxTiO3 perovskites suggested similar mobility for Ba and Ti and a higher mobility for Sr [34, 35-36]. However the lower constrain in the crystal structure can be considered.[37] Taking in account the ratio Mo/Ti could be noted that for small Mo doping the values were lower than the nominal, one with 0.07 and 0.08 for Ba0.5Sr0.5Ti0.9Mo0.1O3 and SrTi0.9Mo0.1O3, respectively. In SrTi0.6Mo0.4O3, a more significant surface segregation of Mo was detected. The cation mobility in doped $BaTiO_3$ was related, by Rahaman et al [36] to the presence of dopants with attitude as donors (increased mobility) and acceptor (decreased mobility). In this case the relative amount of Mo(VI)-donor/Mo(IV)-not donor seems not to play a role confirming that Mo(VI) it is only on surface and cannot affect bulk diffusion. The substitution of Ti with Mo seems to reduce the amount of surface oxygen whose atomic % get closer to the nominal one.
The SEM images of Mo-doped samples (SI – Figure S2). All the samples revealed particle homogeneity with an aggregate morphology. This aggregate morphology, composed by particles with a diameter of 100-200nm, was induced probably by the high temperatures involved during the synthesis. It is interesting to notice that Ba0.5Sr0.5Ti0.9Mo0.1O3 shown a slightly bigger particles diameter (200 nm) than the others compounds, although it was prepared at lower temperatures.
The different synthesis condition did not affect the specific surface area which resulted between 4 and 5 m^2/g.
The particle size distributions displayed the presence of two main diameters, 4 and 0.5 μm, for SrTi0.9Mo0.1O3 and SrTi0.6Mo0.4O3, (Figure S3). The d(0.5) of SrTi0.9Mo0.1O3 and SrTi0.6Mo0.4O3 was 4.014 μm and 4.200 μm, respectively.

Sample		Ni	Ba	Sr	Ti	Mo	O	Mo/Ti	Sr/Ti	O/(Sr+Ti+Mo)
$Ba_{0.5}Sr_{0.5}Ti_{0.9}Mo_{0.1}O_3$	XPS		6	7	14	1	72	0.07	0.50	2.57
			21	25	49	4				
	Nominal		10	10	18	2	60	0.11	0.56	1.50
			25	25	45	5				
$SrTi_{0.9}Mo_{0.1}O_3$	XPS			18	12	1	69	0.08	1.50	2.26
				58	40	2				
	Nominal			20	18	2	60	0.11	1.11	1.50
				50	45	5				
$SrTi_{0.6}Mo_{0.4}O_3$	XPS			17	8	8	67	1.00	2.13	2.03
				52	24	24				
	Nominal			20	12	8	60	0.67	1.67	1.50
				50	30	20				
$SrTiO_3$	XPS			23	13		64	-	1.77	1.78
				63	37					
	Nominal			20	20		60		1.00	1.50
				50	50					
$Sr_{0.5}Ba_{0.5}TiO_3$	XPS		6	8	14	-	72	-	0.57	2.57
			20	29	51					
	Nominal		10	10	20		60		0.50	1.50
			25	25	50					
Ni-ST9M1	XPS	10		13	6	1	72	0.17	2.17	2.57
		36		41	21	2				
	Nominal	7		17	15	2	59	0.13	1.13	1.44
		18		41	37	4				
Ni-ST6M4	XPS	8		12	5	5	71	1.00	2.40	2.45
		29		36	17	17				
	Nominal	7		17	10	7	59	0.70	1.70	1.44
		18		41	25	16				

Table 2: XPS atomic composition obtained for the Mo doped titanates, $Sr_{0.5}Ba_{0.5}TiO_3$, $SrTiO_3$, and .the Ni-activated nanocomposites.

Catalytic and Electrocatalytic behaviour

Enhancing catalytic activity by doping

Reactivity with CO + O_2

$SrTiO_3$ is not active in CO oxidation or in dry reforming [38] whereas doped ones show almost total CO conversion (Figure 5a) at 700-800°C (operative conditions of SOFCs) The total CO conversion is reached by $SrTi_{0.6}Mo_{0.4}O_3$ at 800 °C, $SrTi_{0.9}Mo_{0.1}O_3$ at the same temperature achieved 93% thus underlying the effect of Mo-doping on catalytic activity. $Ba_{0.5}Sr_{0.5}Ti_{0.9}Mo_{0.1}O_3$ has shown the lower CO conversion (80%).

Beyond the total conversion it is interesting to notice that the ignition temperature follows the order $SrTi_{0.9}Mo_{0.1}O_3$ < $SrTi_{0.4}Mo_{0.6}O_3$ < $Ba_{0.5}Sr_{0.5}Ti_{0.9}Mo_{0.1}O_3$ (Figure S4) and a sort of plateau is observed in $SrTi_{0.9}Mo_{0.1}O_3$ (400-500°C) and $SrTi_{0.4}Mo_{0.6}O_3$ (600-700°C). This drop occurs exactly in the temperature range where Mo(IV) is oxidized to Mo(VI), figure 3. This gives important information regarding the essential role of oxygen in these processes. In agreement with the Mars Van Krevelen mechanism expected for perovskite oxide. [39-41] CO is oxidized by lattice oxygen which is successively restored by added oxygen. The severe reducing conditions, necessary for the material preparation, caused, probably, a sub-surface oxygen depletion. When the high temperatures allowed oxygen restoration into the structure and therefore the oxygen ion mobility, the activity received a boost.

A relevant contribution is also due to the surface active oxygen species responsible, at the lower temperature, for a suprafacial mechanism. For undoped and doped $LaCoO_3$, Pinto et al. [42] observed the prevalence of the suprafacial versus intrafacial mechanism until 350°C. The suprafacial activation is probably un-favoured by the stability of Mo(VI).

The compound with the higher amount of Mo is characterized by the larger oxygen consumption (see TPO results) and by the greater improvement in performance, pointing out that the surface (XPS) and bulk (XRD) segregated molybdenum can become active when highly oxidized.

The lower performance was observed on $Ba_{0.5}Sr_{0.5}Ti_{0.9}Mo_{0.1}O_3$ with an ignition temperature of 500 °C but with the absence of an activation step. This is in agreement with the minor oxygen consumption and lower oxygen mobility of $Ba_{0.5}Sr_{0.5}Ti_{0.9}Mo_{0.1}O_3$ which makes difficult the sub-surface oxygen deficiency correction. XPS quantitative analysis, table 2, shows a superior amount of surface hydroxyl groups, which agrees with the lower oxygen adsorption (for which active sites, such as oxygen vacancies or Lewis acidic sites are necessaries) and exchange capability (due to the low bulk mobility).

Low mobility at the grain boundaries can contribute to the low oxygen mobility. Reduced grain boundaries mobility has been observed by several authors and confirmed to be enhanced by aliovalent doping [43]

Reactivity toward methane: Dry reforming

Methane dry reforming (MDR) is an endothermic reaction of high scientific and industrial importance that requires very high temperature [44-47]. In spite of being studied from 1888 it is not yet considered an industrially mature process, also because of the C-poisoning and sintering of the catalysts (mainly based on Ni). Moreover, the implementation of MDR

directly in SOFCs could considerably increase the total efficiency, e.g. due to the heat transfer, and drops the complexity of final device.

Among all the samples, only $SrTi_{0.9}Mo_{0.1}O_3$ show activity at 800 °C, reaching about 58% of CH_4 and 53% of CO_2 conversion, figure 5b. The activity started at around 625 °C with a conversion linear with temperature. The catalyst was kept at 800°C under working condition for 6 hours without showing decrease of catalytic performance (Figure 5c).

Several aspects affect the performances of catalyst: the strong interaction between supporting and active phases, the dispersion and size of active phase, the basicity, the reducibility, the oxygen exchange capability, porosity and specific surface area [48] The mechanism of methane dry reforming has been investigated on several catalysts [49-51]. In general, four steps are considered: 1. Dissociative adsorption of methane: which is the rate determining step and should be favoured by step active sites; 2. Dissociative adsorption of CO_2: which is generally considered fast particularly on metal-support interface. 3. Hydroxyl groups formation, 4. Intermediates oxidation and desorption: surface oxygen is considered responsible of the conversion of CHx –groups adsorbed on the surface in CO and H_2.

The reactivity of the $SrTi_{0.9}Mo_{0.1}O_3$ can be explained by considering the surface composition. Polo-Garzon et al [52] observed a marked effect of the perovskite surface composition and segregation phenomena on catalytic activity. In particular, they investigated the interaction and activation of methane on several $SrTiO_3$ samples obtained by means of different preparation procedures and subjected to different post-synthetic treatments. The obtained results, supported by DFT calculations, indicate that the concentration of Sr at the top layers is proportional to the rate of methane combustion; DFT simulations showed that Sr step surfaces provide the lowest activation barrier for methane dissociation. In the present case XPS indicated that the higher atomic % of Sr are in $SrTi_{0.9}Mo_{0.1}O_3$ only $SrTi_{0.6}Mo_{0.4}O_3$ (18 and 17%, respectively) and this suggest that, beside Sr, Mo also plays a role but the interaction with methane seems to be effective only when Mo is inserted into the perovskite cell.

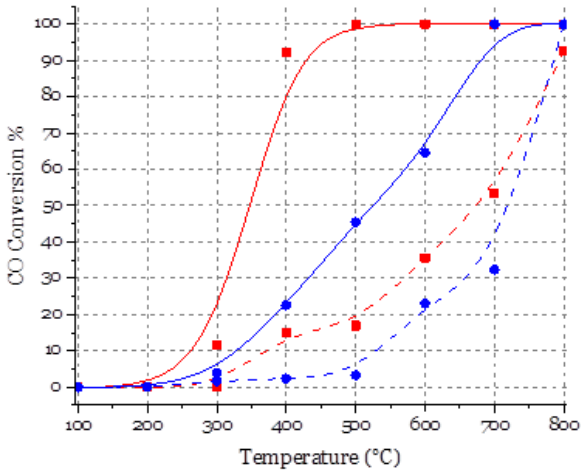

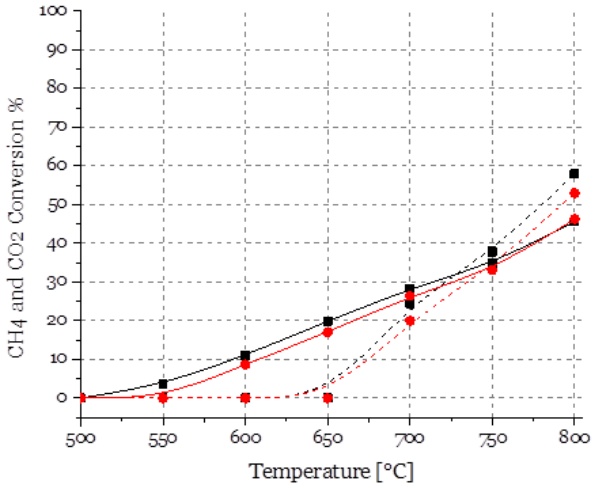

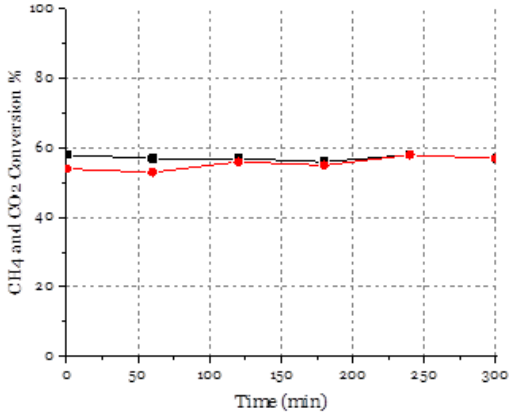

Figure 5 a) CO conversion as a function of temperature for $SrTi_{0.9}Mo_{0.1}O_3$ (Red), $SrTi_{0.4}Mo_{0.6}O_3$ (Blue),. b) $SrTi_{0.9}Mo_{0.1}O_3$: 2 %CH_4 + 2 %CO_2. % Conversion in CH_4+CO_2 (stoichiometric) from 500 °C to 800 °C. CH_4 (black) and CO_2 (Red). c) $SrTi_{0.9}Mo_{0.1}O_3$: 2 %CH_4 + 2 %CO_2. % Conversion in CH_4+CO_2 (stoichiometric) at 800 °C for kept for 300 minutes. CH_4 (black) and CO_2 (Red).

By means of a NAPPES study K. Prabhakar Reddy et al. observed reversible changes in electronic structure of Mo-oxides, related with the presence of Mo(V) necessary to assure the co-existence of Mo(IV) and Mo(VI) and capable of originating now electronic states below the Fermi energy. capable of marked effect on catalytic and electro catalytic behaviour [53 These states could contribute to the weakening of C-H bond. Another role surely played by Mo is in decreasing the C-poisoning: the anti-coking effect of this element was observed, as an example, by Siahvashi et al. in the propane dry reforming [54] and by Neofytidis et al. in a Solid Oxide Fuel Cell operating with methane internal reforming [55] In $SrTi_{0.6}Mo_{0.4}O_3$ molybdenum is also segregated outside the perovskitic cell and cannot contribute to enforce the Mo(IV)/Mo(VI) redox couple. Moreover it is probable that a specific amount of cation is necessary because the activation of CH_4 by Mo-containing sites is not always favourable, depending on the possibility to alloy with other cations originating un-active sites.[56

Enhancing reactivity through nickel deposition

The aim of the Ni (0.3mol%)/SrTi1-xMoxO3 nanocomposites is to make use of the attitude of Mo to bind oxygen to help keeping Ni in elemental state. This should be helpful both for catalysis activity and conductivity (fundamental in SOFC electrodes).

TPR analysis revealed the successful Ni deposition showing the presence of 0.28 and 0.30 mol/mol respectively for Ni/SrTi0.9Mo0.1O3 and Ni/SrTi0.6Mo0.4O3. The signals are centred at 400 and 550°C (Figure S5) and correspond to the two steps reduction of Ni(II). The amount of Ni on surface (XPS, table 3) is higher than the nominal one in Ni/SrTi0.9Mo0.1O3. and almost corresponding to the nominal one in Ni/SrTi0.6Mo0.4O3; the quantitative results suggest the absence of diffusion phenomena, the peak positions correspond to Ni(II). Ni deposition does not affect the Mo/Ti atomic ratio but causes a slight increment of Sr. On other hand a larger amount of oxygen was detected (O/(Sr+Ti+Mo) atomic ratio increases from 2.2 to 2.6).
In figure 5a the results of CO conversion of Ni impregnated compounds vs as prepared SrTi0.9Mo0.1O3 and SrTi0.6Mo0.4O3 are reported. The deposition of 30% mol/mol of Ni greatly increases the catalytic activity: the ignition temperature of SrTi0.9Mo0.1O3 is reduced more than 100 °C and achieved total CO conversion at 500 °C; SrTi0.6Mo0.4O3 shows an ignition temperature around 200 °C and its able to reach the total CO conversion at 700 °C. Both the catalysts did not display the plateau suggesting that oxygen lacking is not a limiting step. This agrees with capability of Ni to facilitate CO chemisorption.

The reactivity towards methane dry reforming was performed on Ni/SrTi0.9Mo0.1O3 and Ni/SrTi0.6Mo0.4O3, but only Ni/SrTi0.9Mo0.1O3 shown reactivity, figure 7b. Ni impregnation does not increase the total CH_4 conversion but causes the decrease of the ignition temperature from 625 °C to 500 °C.. The results underline that the addition of Ni improves the catalytic activity by allowing the methane and carbon dioxide molecules activation at lower temperature In this case, being Ni surface deposited, the amount of Sr revealed by XPS is lower so the improved activation has to be attributed to the role played by Ni. [50] The positive effect of Ni was already observed on $SrTiO_3$-based catalysts [57]; both the CO_2 activation due to the deposited Ni and the CH_4 activation due to the Ni/perovskite interface can be responsible of the increased reactivity. The catalyst was kept at 800 °C under working condition for 6 hours showing only a small decrease in the conversion after the first hour, 41% CH_4 and 38% CO_2. Usually the catalytic performance of Ni-based catalyst greatly decrease due to the well know carbon formation induced by the presence of Ni [58-59]. In our nanocomposite catalyst this loss is limited because of the de-coking action of molybdenum [55, 56].

Enhancing electrochemical performance by Ni infiltration

The electrochemical investigation (EIS) was carried on SrTi0.9Mo0.1O3, Ni/SrTi0.9Mo0.1O3 and Ni/SrTi0.6Mo0.4O3. The selection was based on results obtained by catalytic tests in which the Ba doped compound exhibits the lower performance.
The SOFC cells are the following:

SrTi0.9Mo0.1O3/GDC/YSZ/GDC/SrTi0.9Mo0.1O3
Ni@SrTi0.9Mo0.1O3/GDC/YSZ/GDC/ Ni@SrTi0.9Mo0.1O3
Ni@SrTi0.6Mo0.4O3/GDC/YSZ/GDC/ Ni@SrTi0.6Mo0.4O3

The GDC buffer layer was necessary to avoid ion diffusion and improve compatibility between the electrolyte (YSZ) and the electrode (See Supporting Information – Figure S6)
The success of infiltration was confirmed by the SEM investigation carried out on the final pellets. Figure 6 shows the homogeneous dispersion of Ni particles on the backbone of SrTi0.9Mo0.1O3 and SrTi0.6Mo0.4O3 respectively. SrTi0.6Mo0.4O3 shown a higher porosity and smaller Ni particle diameters (the average diameter is 20-30 nm) compared with SrTi0.9Mo0.1O3 (about 100nm particle diameters). This behaviour was observed to be reproducible suggesting the contribution of backbone to the particles formation.
Area Specific Resistance (ASR) values have been obtained by Nyquist plots through a model circuit fitting – Figure S7)
In figure 7 the evolution of ASR versus the temperature from 500 °C to 830 °C for the samples SrTi0.9Mo0.1O3, Ni-SrTi0.9Mo0.1O3 and Ni-SrTi0.6Mo0.4O3 can be observed.
The best result, 0.85 Ω·cm2, was obtained with SrTi0.6Mo0.4O3 infiltrated with 15%wt of Ni at 830°C. The value found is two orders of magnitude better than the sample SrTi0.9Mo0.1O3 without Ni infiltration (27.2 Ω·cm2) and 0.57 Ω·cm2 less than the sample Ni/SrTi0.9Mo0.1O3. These results displayed that Ni particles on SrTi1-xMoxO3 can greatly improve the performances.

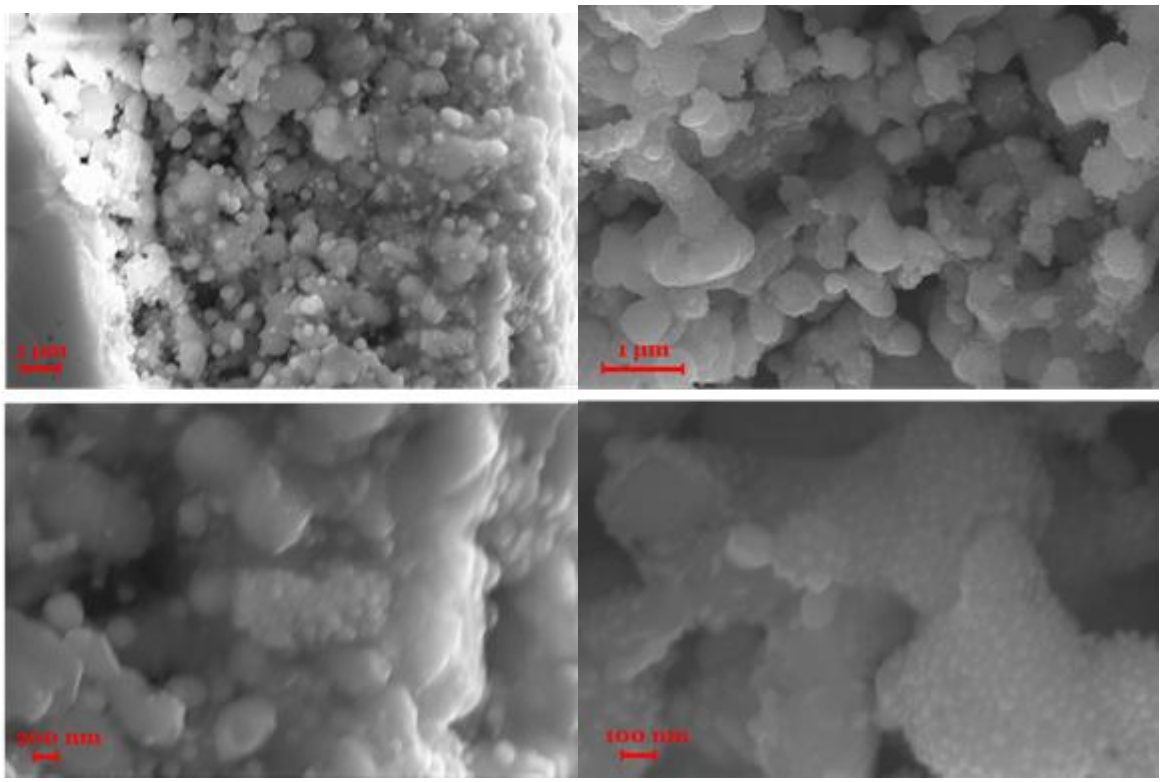

Figure 6: SEM images of Ni/SrTi0.9Mo0.1O3 (left) and Ni/SrTi0.6Mo0.4O3 (right) treated at 1300 °C

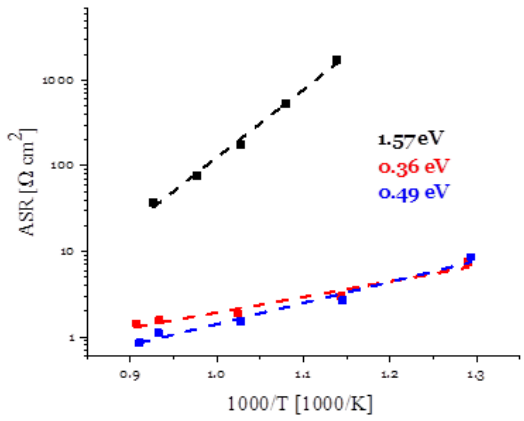

Figure 7. Area specific resistance (ASR) Arrhenius plot for: $SrTi_{0.9}Mo_{0.1}O_3$ (black), $Ni/SrTi_{0.9}Mo_{0.1}O_3$ (red) and $Ni/SrTi_{0.6}Mo_{0.4}O_3$ (blue).

Ni infiltration greatly decrease the Ea for SrTi0.9Mo0.1O3 dropping the value from 1.57 eV to 0.36 eV which is even better than the Ea determined for Ni/SrTi0.6Mo0.4O3 (0.49 eV). With the purpose of understanding which processes were involved in the polarization loss of Ni/SrTi0.9Mo0.1O3 and Ni/SrTi0.6Mo0.4O3, the impedance spectra were fitted allowing to calculate the capacitance of each contributions, Ce, and to distinguish the processes, [60]

The data analysed, for both the symmetric cells, suggested two large contributions to the capacity in the range 10^{-2}-10 F (Figure 8). Their value suggests to attribute them to electrode processes. [60-61]. The comparison with literature suggest that their origin is in the low electro-catalytic performance of titanates [62]. The two contributions in fact were probably related to the reactions occurred on three phase boundaries formed between Ni and the backbone (smaller contribution), and the reactions occurred on perovskites surface (larger contribution).

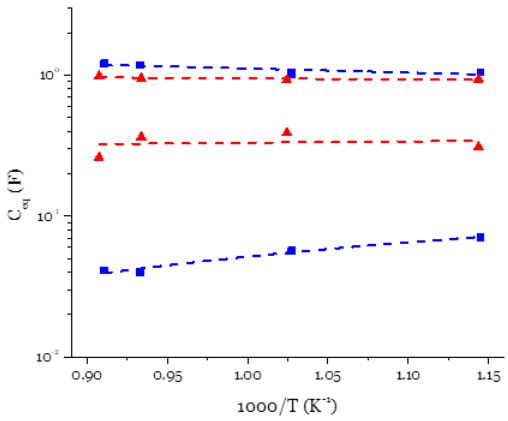

Figure 8: Arrhenius plot of the capacitances for Ni/SrTi0.9Mo0.1O3 (red) and Ni/SrTi0.6Mo0.4O3 (blue).

The absence of the electrode/electrolyte charge transfer at high temperature indicated that electrochemical reactions on the surface could be the rate determining step of the electrode [61]. Impedance spectra, as a function of temperatures, suggest that there not significant changes in microstructures or compositions or at interfaces is taking place at the tested conditions (830 °C under 5% dry H2/Ar) [63].

CONCLUSIONS

In this work new Mo-doped and Ba-doped $SrTiO_3$ (x= 0.5, 1) based materials were developed and optimized paying particular attention to the synthesis and characterization. These new materials have been tested as catalysts (CO oxidation, methane dry reforming) and electro catalysts (anode for solid oxide fuel cells directly feed with bio-gas). Materials design was carried out paying particular attention to avoid critical raw materials (CRM)

High crystalline purity on all the compounds required an accurate optimization to define the peculiar pO_2 pressure conditions. The desired phases of $SrTi_{0.9}Mo_{0.1}O_3$, $SrTi_{0.6}Mo_{0.4}O_3$ and $Ba_{0.5}Sr_{0.5}Ti_{0.9}Mo_{0.1}O_3$ were achieved through reductive thermal treatments (1200 °C under 5% wet H2/Ar the Mo-doped and 1000 °C under 5% H2/Ar with ethanol-water vapour $Ba_{0.5}Sr_{0.5}Ti_{0.9}Mo_{0.1}O_3$).

The high temperatures involved in the compounds preparations could be the causes of the large particle diameters observed with the SEM images and with laser diffusion technique, d(0.5) nearly 4µm. SEM images also suggest a partial sinterization between the starting particles.

The stability tests (TPR/TPO) performed on samples powders have revealed high stability of $SrTi_{0.9}Mo_{0.1}O_3$, $SrTi_{0.6}Mo_{0.4}O_3$ and $Ba_{0.5}Sr_{0.5}Ti_{0.9}Mo_{0.1}O_3$ under reductive conditions (5% H2/Ar up to 900 °C) but traces of insulating phases, $SrMoO_4$ and $BaMoO_4$ depending from the A-site cations, appear above 500 °C under oxidising conditions. This behaviour does not affect the performance under working conditions but might induce particular attention during a cell preparation. $SrTi_{0.9}Mo_{0.1}O_3$ shows a total structure restoration after TPO/TPR treatments.

All the materials were highly active towards CO oxidation under working temperature condition (total CO conversion for $SrTi_{0.6}Mo_{0.4}O_3$, 93% for $SrTi_{0.9}Mo_{0.1}O_3$ and 80% for $Ba_{0.5}Sr_{0.5}Ti_{0.9}Mo_{0.1}O_3$). Among the samples tested, $SrTi_{0.9}Mo_{0.1}O_3$ was the only material that reached a decent activity versus methane dry reforming, 58% of CH_4 and 53% of CO_2 conversion at 800 °C. The material was kept in working condition for several hours without showing decreasing in conversion. The curious activity observed is probably due to a synergic effect between Ti and Mo (Ti/Mo = 9/1) which was not observed on the other Mo-doped compounds. The higher stability and the interesting reactivity observed for $SrTi_{0.9}Mo_{0.1}O_3$ and $SrTi_{0.6}Mo_{0.4}O_3$ had encouraged focusing on these systems as anode for solid oxide fuel cell. With the purpose to enhancing the catalytic behaviour, nickel deposition (30%mol) on $SrTi_{0.9}Mo_{0.1}O_3$ and $SrTi_{0.6}Mo_{0.4}O_3$ was carried out. As expected the CO oxidation received a remarkable boost achieving the total conversion at 500 °C and 700 °C respectively for $SrTi_{0.9}Mo_{0.1}O_3$ and $SrTi_{0.6}Mo_{0.4}O_3$. Again, only $Ni/SrTi_{0.9}Mo_{0.1}O_3$ showed a decent activity toward methane dry reforming. Although the CH_4 conversions slightly decrease from 58% to 41% and the ignition temperature drops (from 650 °C to 500 °C). The reactivity tests confirm that although some optimization steps are still required such as synthesis and the nickel particles dispersion. $Ni/SrTi_{0.9}Mo_{0.1}O_3$ could be used as material for the methane dry reforming.

The realization of symmetric cells and impedance spectra investigation has demonstrated the feasibility to use $SrTi_{0.9}Mo_{0.1}O_3$ and $SrTi_{0.6}Mo_{0.4}O_3$ infiltrated with 15wt% with nickel as anode for solid oxide fuel cell. The lowest ASR, 0.85 $\Omega \cdot cm^2$, was achieved at 830 °C with $Ni/SrTi_{0.6}Mo_{0.4}O_3$.

REFERENCES

[1] Collignon, C.; Lin, X.; Rischau, C.W.; Fauque, B.; Behnia, K. Ann. Rev. Cond. Matter Phys Vol 10. Sachdev, S; Marchetti, M.C. Metallicity and Superconductivity in Doped Strontium Titanate Eds.; 2019 Book Series: Annual Review of Condensed Matter Physics Vol. 10 pp 25-44
DOI: 10.1146/annurev-conmatphys-031218-013144

2 Adnan, M.A.B.; Arifin, K.; Minggu, L.J.; Kassim, M.B. Titanate-based perovskites for photochemical and photoelectrochemical water splitting applications: A review *Int. J. Hydrogen Energy* **2018**, *43*, 23209-23220
Published: DEC 27 2018,

[3] Tzu, H.C.; Hao, L.; Takashi, H.; Yosuke G.; Tsuyoshi T.; Masao, K.; Tsutomu M.; Kazunari D., *ACS Catal.* **2018**, *8*, 2782–2788 Efficient Photocatalytic Water Splitting Using Al-Doped $SrTiO_3$ Coloaded with Molybdenum Oxide and Rhodium–Chromium Oxide

4 Tejuca, L.G.; Fierro, J.L.G.; Tascón J.M.D., Structure and reactivity of perovskite-type oxides, *Adv. Catal.* **1989**, 36, 237-327;

5 Peña M.A., Fierro J.L.G. Chemical Structures and Performance of Perovskitic oxides *Chem. Rev*. **2001**, *101*, 1981-2018.

6. Savaniu C. D., Irvine J. T. S., La-doped $SrTiO_3$ as anode material for IT-SOFC, *Solid State Ionics*, **2011**, *192*, 491–493.

7. Gorte R. J., Kim H., Vohs J. M. Novel SOFC Anodes for the Direct Electrochemical Oxidation of Hydrocarbons, *J. Power Sources*, **2002**, 106, 10-15.

8. Orera A. Slater P. R. New chemical systems for solid oxide fuel cells, *Chem. Mater.*, **2010,** *22*, 675–690.

9. Yi, H. Li, H. Chen, R. Zhao, and X. Jiang, Preparation and characterization of La and Cr co-doped $SrTiO_3$ materials for SOFC anode, *Ceram. Int.*, **2013**. *39*, 347–352.

10 Vincent A., Luo J. L., Chuang K. T., Sanger A. R., Effect of Ba doping on performance of LST as anode in solid oxide fuel cells, *J. Power Sources*, **2010**. *195*,769–774.

[11] Hou X., Marin-Flores O., Kwon B. W., Kim J., Norton M. G., Ha S., Gasoline-fueled solid oxide fuel cell with high power density, *J. Power Sources*, **2014**. *268*, 546–549.

[12] Marrero-López D., Peña-Martínez J., Ruiz-Morales J. C., Martín-Sedeño M. C., Núñez P., High temperature phase transition in SOFC anodes based on $Sr_2MgMoO_{6-\delta}$, *J. Solid State Chem.*, **2009**, *182*, 1027–1034.

[13] He B., Wang Z., Zhao L., Pan X., Wu X., Xia C., Ti-doped molybdenum-based perovskites as anodes for solid oxide fuel cells, J. Power Sources, **2013**,. *241*, 627–633.

[14] Graves C.; Martinez, L., Sudireddy, B.R. . High performance nano-ceria electrodes for solid oxide cells *ECS Trans*. **2016**, *72* 183-192.

[15] Vasala S., Yamauchi H., Karppinen M., Role of $SrMoO_4$ in Sr_2MgMoO_6 synthesis, *J. Solid State Chem.*,. **2011**, *184*, 1312–1317.
[16] Dos Santos-Gómez L., León-Reina L., Porras-Vázquez J. M., Losilla E. R., Marrero-López D., Chemical stability and compatibility of double perovskite anode materials for SOFCs, *Solid State Ionics*, **2013,** *239*, 1–7.
[17] Marrero-López D., Peña-Martínez J. Ruiz-Morales J.C., Gabás M., Núñez P., Arand M.A.G., Ramos-Barrado J.R., Redox behaviour, chemical compatibility and electrochemical performance of Sr_2MgMoO_6 - δ as SOFC anode, *Solid State Ionics*, **2010**, *180,* 1672–1682.
[18] Yang L. C., Gao Q. S., Tang Y., Wu Y. P., Holze R., MoO_2 synthesized by reduction of MoO_3 with ethanol vapor as an anode material with good rate capability for the lithium ion battery, *J. Power Sources*, **2008**. *179*, 357–360.
[19] Takehira K., Shishido T., Kondo M., Partial Oxidation of CH_4 over $Ni/SrTiO_3$ Catalysts Prepared by a Solid-Phase Crystallization Method, **2002**, . *316*, 307–316.
[20] Thallada Bhaskar, Kondakindi Rajender Reddy, Chinthala Praveen Kumar, Mamidanna R.V.S. Murthy, Komandur V.R. Chary Characterization and reactivity of molybdenum oxide catalysts supported on zirconia *Appl. Catal. A: General* **2001**, *211*, 189–201.
21. Kubo, W. Ueda, Catalytic behavior of AMoOx (A = Ba, Sr) in oxidation of 2-propanol, *Mater. Res. Bull.*, **2009**, *44*, 906–912.
22 Martínez-Coronado R., Alonso J. A., Aguadero A., Fernández-Díaz M. T., New $SrMo_{1-x}Cr_xO_{3-\delta}$ perovskites as anodes in solid-oxide fuel cells, *Int. J. Hydrogen Energy*, **2014**, 39, 4067–4073.
23 Ura B., Trawczyński J., Kotarba A., Bieniasz W., III án-Gómez M.J., Bueno-López A., López-Suárez; Effect of potassium addition on catalytic activity of $SrTiO_3$ catalyst for diesel soot combustion, *Appl. Catal. B Environ.*, **2011,** *101*, 169–175.
24 Yang W., X-ray photoelectron spectroscopy and electrical properties studies of La_2O_3 -doped strontium titanate ceramics prepared by sol-precipitation method, *J. Mater. Sci*. **1999**, *4*, 3533–3544.
25. Nagarkar V., Searson P. C., Gealy III F. D., Effect of surface treatment on $SrTio_3$: An x-ray photoelectron spectroscopic study, *J. Appl. Phys*. **1991**, *69*, 459.
26 Tsunekawa S., Ito S., Mori T., Ishikawa K., Li Z., Kawazoe Y., Critical size and anomalous lattice expansion in nanocrystalline $BaTiO_3$ particles, *Phys. Rev. B,* **2000**, *62*, 3065-3070.
27 Wegmann M., Watson L., Hendry A. XPS Analysis of Submicrometer Barium Titanate Powder, *J. Am. Ceram. Soc*. **2008**, *87*, 371–377.
28. Ellefson C. A., Marin-Flores O., Ha S., Norton M. G., Synthesis and applications of molybdenum (IV) oxide, *J. Mater. Sci.*, **2012,** 47, 2057–2071.
29. Li J., Lv T., Hou N., Li P., X. Yao, L. Fan, T. Gan, Y. Zhao, Y. Li; Molybdenum substitution at the B-site of lanthanum strontium titanate anodes for solid oxide fuel cells, *Int. J. Hydrogen Energy*, **2017**, 42, 22294-2230.
30 Choi J., Thompson L. T., XPS study of as-prepared and reduced molybdenum oxides, *Appl. Surf. Sci*. **1996**, *93*, 143–149.
31 Verhoeven J.A.Th., Doveren H.Van, An XPS investigation of the interaction of CH_4, C_2H_2, C_2H_4 and C_2H_6 with a barium surface, Surf. Sci. **1982,** *123*, 369–383.
32 Hanawa T., Ota M., Calcium phosphate naturally formed on titanium in electrolyte solution, *Biomaterials*, **1991**, *12*, 767-774
33 Zou J., Schrader G. L., Multicomponent Thin Film Molybdate Catalysts for the Selective Oxidation of 1 , 3-Butadiene, J. Catal. **1996**, 686, 667–686.
[34] Yoo H-I., Lee C.-E., De Souza R.A., Martin M. Equal mobility of constituent cations in $BaTiO_3$ *Appl. Phys Lett*., **2008**, *92*, 25213-1-3
35 Lee C.-E. Yoo H.-I., Ba/Ti ratio effect on oxygen re-equilibration kinetics of donor-doped $BaTiO_3$ *Solid State Ionics*, **2008**, *179,* 338–334
36 Saha S., Krupanidhi B.K. Microstructure related influence on the electrical properties of pulsed laser ablated $(Ba,Sr)TiO_3$ thin films *J. Appl. Phys*, **2000**, *88*, 3506-3513.
[37] Shannon R. D., Revised effective ionic radii and systematic studies of interatomic distances in halides and chalcogenides, *Acta Crystallogr. Sect. A*, **1976,** 32, 751–767.
[38] Glisenti A., Natile M.M., Carlotto S., Vittadini A. Co- and Cu-Doped Titanates: Toward a New Generation of Catalytic Converters, *Catal. Lett*. **2014**, *144*, 1466-1471.
39 Pena M. A., Fierro J. L. G., Chemical structures and performances of perovskite oxides, *Chem. Rev*., **2001**, *101*, 1981–2017.
40 Royer S., Duprez D., Kaliaguine S., Oxygen mobility in $LaCoO_3$ perovskites, *Catal. Today*, **2006**, *112*, 99–102.
41 Mars P., van Krevelen D. W., Oxidations carried out by means of vanadium oxide catalysts, *Chem. Eng. Sci.,* **1954,** *3*, 41–59.
42 D. Pinto, A. Glisenti, Pulsed reactivity on $LaCoO_3$-based perovskites: a comprehensive approach to go inside CO oxidation mechanism and the effect of dopants, *Catal. Science and Technology,* **2019**, *9,* 2749-2757.
[43] Rahaman M.N., Manalert R., Grain Boundary Mobility of $BaTiO_3$ doped with Aliovalent Cations, *J. Europ. Ceramic Soc*. **1998**, *18*, 1063-1071

44 Pakhare D., Spivey J., A review of dry (CO_2) reforming of methane over noble metal catalysts, *Chem. Soc. Rev*., **2014**, *43*, 7813-7837,
45 Jang W.J., Shim J.-O., Kim H.-M., Yoo S.-Y., Roh H.-S.; A review on dry reforming of methane in aspect of catalytic properties; *Catal. Today*, **2019,** *324*, 15-26.
46 Wang Y., Yao L., Wang S., Mao D., Hu C. Low-temperature catalytic CO_2 dry reforming of methane on Ni-based catalysts: a review *Fuel Processing Technology,* **2018**, *169*, 199-206.
47 Abdel Karim Aramouni N., Touma J. G., Abu Tarboush B., Zeaiter J., Ahmad M.N., Catalyst design for dry reforming of methane: analysis review *Renew. Sustainable Energy Reviews* **2018,** *82*, 2570-2585
[48] Jang W.-J., Shim J.-Oh., Kim H.-M., Yoo S.-Y., Roh H.-S., A review on dry reforming of methane in aspect of catalytic properties *Catal. Today,* **2019**, *324*, 15-26.
49 Papadopoulou C., Matralis H., Verykios X., Utilization of Biogas as a Renewable Carbon Source: Dry Reforming of Methane in Catalysis for Alternative Energy Generation LGuczi L., Erdöhelyi A. Eds. Springer New York, 2012. pp 57-127
50 Kumar N., Kanitkar S., Wang Z., Haynes D., Shekhawat D., Spivey J.J.; Dry reforming of methane with isotopic gas mixture over Ni-based pyrochlore catalyst *Int. J. Hydrogen Energy* **2019**, *44*, 4167-4176

51 Bachiller-Baeza B., Mateos-Pedrero C., Soria M.A., Guerrero-Ruiz A., Rodemerck U., Rodríguez-Ramos I., Transient studies of low-temperature dry reforming of methane over Ni-CaO/ZrO2-La2O3 *Appl. Catal. B Environ.* **2013**, *129*, 450-459
[52] Polo-Garzon F., Fung V., Liu X., Hood Z.D., Bickel E.E., Bai L., Tian G., G.S. Foo G.S., Chi M., Jiang D., Wu Z.; Understanding the Impact of surface reconstruction of perovskite catalysts on CH4 activation and combustion *ACS Catal* **2018**, *8* 10306-10315
[53] Prabhakar Reddy K., Mhamane N. B., Kumar Ghosalya M., Gopinath C. S.; Mapping valence band and interface electronic structure changes during the oxidation of Mo to MoO3 via MoO2 and MoO3 to MoO2: a NAPPES study *J. Phys. Chem. C.* **2018**, *122*, 23034-23044.
[54] Siahvashi A., Chesterfield D., Adesina A.A.; Propane CO2 (dry) reforming over bimetallic Mo-Ni/Al2O3 catalyst *Chem. Eng. Science* **2013**, *93*, 313-325.
[55] Neofytidis Ch., Dracopoulos V., Neophytides S.G., Niakolas D.K.; Electrocatalytic performance and ccarbon tolerance of ternary Au-Mo-Ni/GDC SOFC anodes under CH4-rich Internal Steam Reforming conditions; *Catal. Today* **2018**, *310* 157-165
[56] Yao L., Galvez M.E., Hu C., Da Costa P.; Mo-promoted Ni/Al2O3 catalyst for dry reforming of methane *Int. J. Hydrogen Energy* **2017**, *42*, 23500-23507
57 Kwon B.W., Oh J.H., Kim G. S., Yoon S.P., Han J., Nam S.W., Ham H.C.; The novel perovskite-type Ni-doped Sro.92Yo.08TiO3 catalyst as a reforming biogas (CH4+CO2) for H2 production; *Appl Energy* **2018**, *227*, 213-219
58 Usman M., Wan Daud W. M. A., Abbas H. F., Dry reforming of methane: Influence of process parameters—A review, Renew. *Sustain. Energy Rev*., **2015**, *45*, 710–744.
59 Pérez-Camacho M. N., Abu-Dahrieh J., Goguet A., Sun K., Rooney D., Self-cleaning perovskite type catalysts for the dry reforming of methane, *Chinese J. Catal.*, **2014**, *35*, no. 8, 1337–1346.
60 Dailly J., Fourcade S., Largeteau A., Mauvy F., Grenier J. C., Marrony M., Perovskite and A2MO 4-type oxides as new cathode materials for protonic solid oxide fuel cells, *Electrochim. Acta,* **2010**, *55*, 5847–5853
61 Du Z., Zhao H., Yang C., Shen Y., Yan C., Optimization of strontium molybdate based composite anode for solid oxide fuel cells, *J. Power Sources*, **2015**, *274*, 568–574.
62 Zhou X, Yan N., Chuang K. T., Luo J., Progress in La-doped SrTiO3 (LST)-based anode materials for solid oxide fuel cells, *RSC Adv*., **2014**, *4*, 118-131.
63 Hayashi H., Thermal expansion of Gd-doped ceria and reduced ceria, *Solid State Ionics*, **2000**, *132*, 227–233.